JUSTC

Article

http://justc.ustc.edu.cn

Received: May 21, 2024; Accepted: August 07, 2024

Unbiased test of the hyperon *CP* violation in terms of detector resolution at STCF

Ming Xu[1,2] ✉, Liang Liu[1,2], Yupeng Pei[1,2], Xiaorong Zhou[1,2], and Yingchun Zhu[1,2]

[1]*Department of Modern Physics, School of Physical Sciences, University of Science and Technology of China, Hefei 230026, China;*
[2]*State Key Laboratory of Particle Detection and Electronics, University of Science and Technology of China, Hefei 230026, China*

✉Correspondence: Ming Xu, E-mail: xumingname@mail.ustc.edu.cn

Graphical abstract

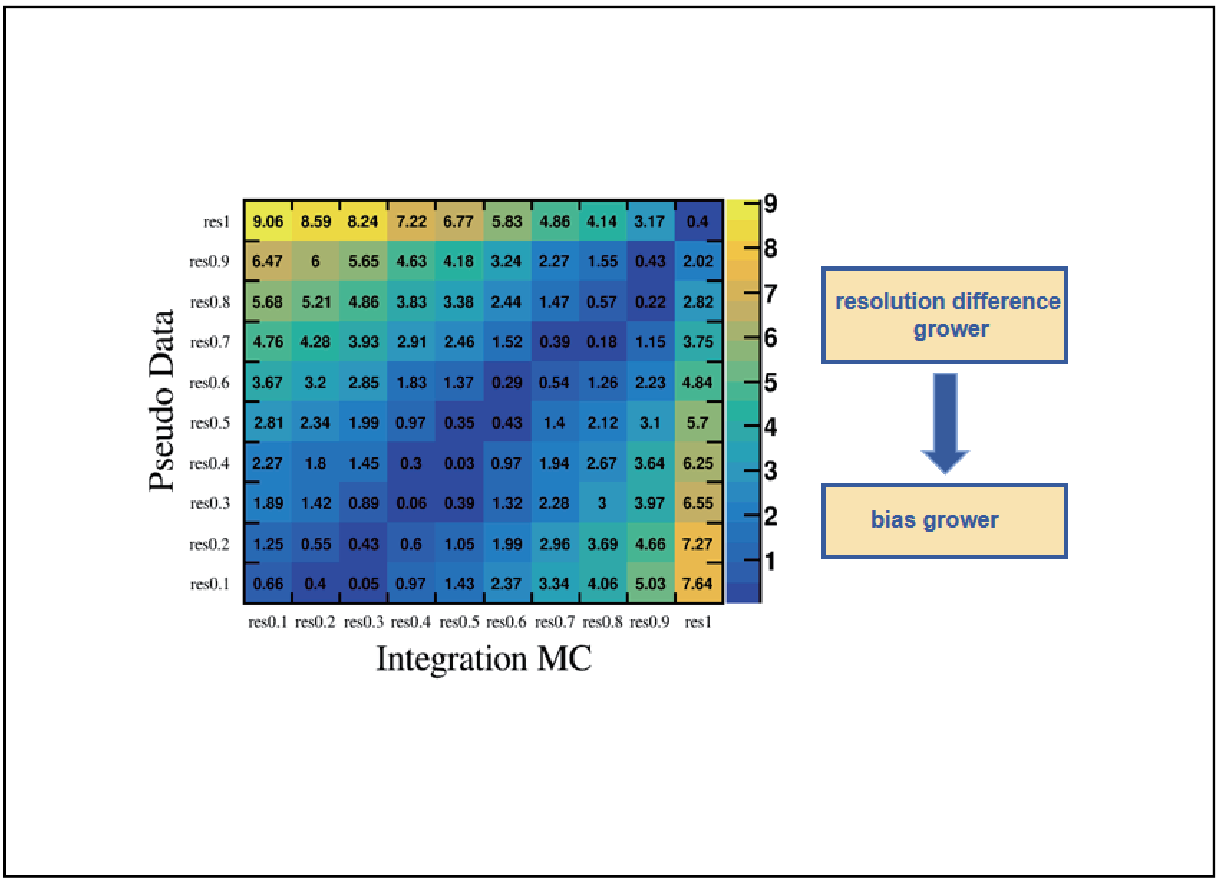

Only when the MC simulation with correct position/momentum resolution compared to data, the IO on the parameters is unbiased.

Public summary

- In the probe of *CP* violation in hyperon decays at future STCF, the expected statistical sensitivity of hyperon decay parameters will reach a level of $O(10^{-4})-O(10^{-5})$, making systematic uncertainties a key limited factor.
- Refined vertex fitting method that accurately accounts for track energy loss effect can effectively reduce the corresponding systematic uncertainties.
- A biased simulation of detector resolution will introduce deviation of the decay parameters from true physical value.

Citation: Xu M, Liu L, Pei Y P, et al. Unbiased test of the hyperon *CP* violation in terms of detector resolution at STCF. *JUSTC*, **2025**, 55(4): 0405.
CSTR: 32290.14.JUSTC-2024-0072. DOI: 10.52396/JUSTC-2024-0072

Article
http://justc.ustc.edu.cn
Received: May 21, 2024; Accepted: August 07, 2024

Unbiased test of the hyperon *CP* violation in terms of detector resolution at STCF

Ming Xu[1,2] ✉, Liang Liu[1,2], Yupeng Pei[1,2], Xiaorong Zhou[1,2], and Yingchun Zhu[1,2]

[1]Department of Modern Physics, School of Physical Sciences, University of Science and Technology of China, Hefei 230026, China;
[2]State Key Laboratory of Particle Detection and Electronics, University of Science and Technology of China, Hefei 230026, China

✉Correspondence: Ming Xu, E-mail: xumingname@mail.ustc.edu.cn

Cite This: *JUSTC*, **2025**, 55(4): 0405 (7pp)
Read Online

Abstract: The study of the charge conjugation and parity (*CP*) violation of hyperon is the precision frontier for probing possible new *CP* violation sources beyond the standard model (SM). With the large number of quantum entangled hyperon-antihyperon pairs to be produced at Super Tau-Charm Facility (STCF), the *CP* asymmetry of hyperon is expected to be tested with a statistical sensitivity of 10^{-4} or even better. To cope with the statistical precision, the systematic effects from various aspects are critical and need to be studied in detail. In this paper, the sensitivity effects on the *CP* violation parameters associated with the detector resolution, including those of the position and momentum, are studied and discussed in detail. The results provide valuable guidance for the design of STCF detector.

Keywords: BESIII experiment; STCF; hyperon *CP* violation; detector resolution; unbiased test

CLC number: O572.21+2 **Document code:** A

1 Introduction

Principles of symmetry play a crucial role in the frontier of particle physics[1]. Violation of the joint charge conjugation and parity (*CP*) symmetry in fundamental interactions is a key observable for understanding the dynamically generated matter-antimatter asymmetry in the Universe[2]. The discovery of *CP* violation (CPV) in the kaon system helped to establish the Kobayashi−Maskawa (KM) mechanism in the standard model (SM) of particle physics and won the physics Nobel Prize in 1980[3−5]. To date, CPVs have also been observed in both the B meson and the charm meson systems[6,7], which are highly consistent with the SM predictions in terms of magnitude. However, the effects observed in the meson sector are too weak to explain the observed matter-antimatter asymmetry of the universe[8]. The KM mechanism of the SM also predicts a series of CPV phenomena in the baryon sector, which have not yet been observed[9−12]. Therefore, *CP* tests in the baryon sector are regarded as a promising window to search for new physics beyond the SM.

Similar to the case in the kaon mesons, the direct CPV effects in hyperon decays occur through the penguin diagrams in the SM[13]. To generate a *CP* asymmetry, two coherent amplitudes are needed. In $K_L \to \pi^+\pi^-$, the direct CPV arises from the interference of the two amplitudes with iso-spin changes $\Delta I = 1/2$ and $\Delta I = 3/2$ in the S-wave transition[14]. However, in the hyperon weak decay $Y' \to Y\pi$ where Y' and Y denote the initial and final state hyperons, respectively, the direct CPV arises from the interference of amplitudes with S wave and P wave[13]. Therefore, the study of CPV in hyperon decay is a complementary approach in two-body nonleptonic $\Delta S = 1$ transitions.

Three experimental observables are the decay width $\Gamma = \frac{e^2 G_F^2}{\pi}(|S|^2 + |P|^2)$, the decay asymmetry parameters $\alpha = \frac{2\mathrm{Re}(S^* P)}{|S|^2 + |P|^2}$, and $\phi = \arg[(S+P)(S^* - P^*)]$, where G_F is Fermi coupling constant, Re denotes the real part and arg represents extracting the complex phase. It can be constructed with the decay amplitudes of the S-wave and P-wave transitions in hyperon decays[13,15]. According to the above definitions, the decay widths and decay parameters are all *CP*-odd, and can be used to construct CPV observables as follows:

$$\begin{aligned}\Delta_{CP} &= \frac{\Gamma - \bar{\Gamma}}{\Gamma + \bar{\Gamma}},\\ A_{CP} &= \frac{\alpha + \bar{\alpha}}{\alpha - \bar{\alpha}},\\ \Delta\phi_{CP} &= \frac{\phi + \bar{\phi}}{2}.\end{aligned} \tag{1}$$

The SM predicts the CPV of the above observables ranging from $\mathcal{O}(10^{-7})$ to $\mathcal{O}(10^{-3})$, depending on the different CPV observables used[9,10]. Some phenomenological models beyond the SM allow the asymmetry to be increased by orders of magnitude[16], and offer opportunities to discover new physics.

Since 2019, the BESIII experiment has demonstrated its great potential in searching for hyperon CPV in the e^+e^- collider[17]. With the large J/ψ sample collected by the BESIII detector and the large branching fraction of $J/\psi \to Y\bar{Y}$, where $Y\bar{Y}$ denotes hyperon and anti-hyperon pairs, tens of millions of quantum entangled hyperon and anti-hyperon pairs are obtained. Moreover, the hyperon pairs produced in the J/ψ decay are found to be naturally polarized transversely due to the non-zero phase of two helicity amplitudes. In the decay $J/\psi \to Y\bar{Y}$, the transverse polarization of hyperons P_y is expressed as

$$P_y = -\frac{\sqrt{1-\alpha_\psi^2}\sin\theta\cos\theta}{1+\alpha_\psi\cos^2\theta}\sin\Delta\Phi, \tag{2}$$

where α_ψ and $\Delta\Phi$ are the corresponding production parameters and are explained explicitly in Section 3. Table 1 summarizes the branching fraction, α_ψ, $\Delta\Phi$, and the maximum polarization $P_y^{\max}$ of the hyperons produced in J/ψ decay, as well as the latest results of A_{CP} for various hyperons from the BESIII experiment, where the CPV tests are most precise in the world to date although the statistics of hyperons in the BESIII are three orders of magnitude smaller than those of the fixed target experiments. Benefiting from the features of polarization, quantum entanglement, a clean environment, and high precision at the e^+e^- collider, the sensitivity of CPV tests in hyperons is expected to improve significantly. The future e^+e^- facility with much increasing luminosity operating in the τ-charm energy region, Super Tau-Charm Facility (STCF)[18], offers a promising opportunity for breakthroughs in this field.

The proposed STCF will operates at center-of-mass (c.m.) energies from 2 to 7 GeV, with a peak luminosity of 0.5×10^{35} cm$^{-2}\cdot$s^{-1} or even higher. Under the assumption of 60% efficiency in data taking, it is expected to collect more than 1 ab^{-1} data per year, corresponding to around 3.4 trillion J/ψ events with the current designed energy spread of 0.027%.

On the basis of the current design performance of the spectrometer, the statistical sensitivities of the CPV test for the hyperons in the decay $J/\psi \to Y\bar{Y}$ are of the level of $\mathcal{O}(10^{-4})-\mathcal{O}(10^{-5})$, which are comparable to those of SM prediction[24,25]. According to Ref. [25], changes in detector resolution can lead to variations in signal efficiency. Therefore, the systematic uncertainty is crucial for the searches for new physics.

In this paper, we focus on the study of $J/\psi \to \Lambda\bar{\Lambda}$ and $J/\psi \to \Xi^-\bar{\Xi}^+$ and show how the detector resolutions affect the sensitivity of CPV parameters.

2 STCF spectrometer and Monte Carlo simulations

The STCF spectrometer is a general purpose detector designed for an e^+e^- collider. From the interaction point outward, it consists of a tracking system composed of an inner track detector (ITK) and a main draft chamber (MDC), a particle identification (PID) system that consists of a ring imaging Cherenkov (RICH) detector in the barrel region and a detection of internally reflected Cherenkov (DIRC)-like time-of-flight (DTOF) detector in the endcap region, providing 4σ charged K/π separation up to 2 GeV/c, an electromagnetic calorimeter (EMC) with excellent energy resolution of approximately 2.5% for 1 GeV photons and good time resolution of about 300 ps for 1 GeV energy deposits, a superconducting solenoid and a muon detector (MUD) which provides good charged π/μ separation. The detailed conceptual design for STCF spectrometer can be found in Ref. [18].

The detection efficiency and spatial resolution for charged tracks are essential in the studies of the hyperon CPV tests. The charged tracks are detected with the ITK and MDC systems. The ITK consists of three layers of low-material budget silicon or gaseous detectors, with each layer having a material budget of approximately 0.25% X/X_0. The single-hit spatial resolutions in the $r-\phi$ direction and beamline direction are expected to be better than 100 μm and 450 μm, respectively, enabling high detection efficiency for low-momentum tracks. The helium-based MDC is the primary subdetector of the tracking system, providing efficient and precise trajectory measurements for charged particles with a momentum resolution better than 0.5% at 1 GeV/c and the ionization energy loss dE/dx resolution of approximately 6% for electrons from Bhabha scattering.

To study the detector performance, two kinds of Monte Carlo (MC) samples are used. One is the processes $J/\psi \to \Lambda\bar{\Lambda}$ and $J/\psi \to \Xi^-\bar{\Xi}^-$ that are generated based on the BESIII offline software system (BOSS), with full GEANT4 simulation, which is used to study the reconstruction performance of Λ and Ξ^- along with the decay length with current available vertex fit methods. About 5 million $J/\psi \to \Lambda\bar{\Lambda} \to p\pi^-\bar{p}\pi^+$ events and 50 million $J/\psi \to \Xi(\Lambda\pi^-)\bar{\Xi}(\bar{\Lambda}\pi^+) \to p\pi^-\pi^-\bar{p}\pi^+\pi^+$ events are used in this study. The other is the process $J/\psi \to \Lambda\bar{\Lambda}$, which is based on a GEANT4-free fast simulation package[26], which takes the same event generator as the first one, but takes the resolution and efficiency responses for the tracking of final state particles, the PID system and kinematic fit related variables via sampling. Approximately 7.7×10^8 $J/\psi \to \Lambda\bar{\Lambda} \to p\pi^-\bar{p}\pi^+$ events, corresponding to 1 trillion J/ψ, are used in this detector performance test. Since the STCF detector and the corresponding offline software system are in research and development, the later simulation provides a flexible interface for adjusting the performance of each subsystem, which can be used to optimize the detector design according to the physical requirements.

3 Formalism

The decay amplitude of low energy hadron processes can be formulated phenomenologically resorting to the electromagnetic

Table 1. The branching fraction, the production parameters α_ψ and $\Delta\Phi$, and the maximum polarization $P_y^{\max}$ produced in J/ψ decay, the latest results of A_{CP} for various hyperons are summarized.

$Y\bar{Y}$ mode	$\mathcal{B}(\times10^{-3})$[19]	α_ψ	$\Delta\Phi$	$P_y^{\max}$	A_{CP}
$J/\psi\to\Lambda\bar{\Lambda}$	1.89 ± 0.09	0.475 ± 0.003	0.752 ± 0.008	25%	$-0.0025\pm0.0046\pm0.0011$[20]
$J/\psi\to\Sigma^+\bar{\Sigma}^-$	1.07 ± 0.04	-0.508 ± 0.007	-0.27 ± 0.02	16%	$-0.004\pm0.037\pm0.010$[21]
$J/\psi\to\Xi^0\bar{\Xi}^0$	1.17 ± 0.04	0.66 ± 0.06	1.16 ± 0.02	27%	$-0.0054\pm0.0065\pm0.0031$[22]
$J/\psi\to\Xi^-\bar{\Xi}^+$	0.97 ± 0.08	0.59 ± 0.02	1.21 ± 0.05	30%	$0.006\pm0.013\pm0.006$[23]

CSTR: 32290.14.JUSTC-2024-0072
DOI: 10.52396/JUSTC-2024-0072
JUSTC, **2025**, 55(4): 0405

form factors for the implicit understanding of the inner structures of hadrons and the unreliable accuracy when applying QCD sum rules. Taking $J/\psi \to \Lambda\bar{\Lambda}$ as an example, the general formula is expressed as[27]

$$|M(e^+e^- \to \Lambda(\boldsymbol{s}_1)\bar{\Lambda}(\boldsymbol{s}_2))|^2 = \mathcal{K}\boldsymbol{L}\cdot\boldsymbol{K}(\boldsymbol{s}_1,\boldsymbol{s}_2), \tag{3}$$

where $\mathcal{K}$ is a prefactor related to the propagator involving unstable particle J/ψ. $\boldsymbol{L}$ and $\boldsymbol{K}$ are lepton tensor and hadron tensor. And $\boldsymbol{s}_1$, $\boldsymbol{s}_2$ are spin-four vectors for Λ and $\bar{\Lambda}$. $\boldsymbol{L}$ can be directly calculated out and $\boldsymbol{K}$ is embedded in form factors through the hyperon vertex function

$$\Gamma_\mu^\Lambda(p_1,p_2) = -\mathrm{ie}\left[G_\mathrm{M}^\psi\gamma_\mu - \frac{2M}{Q^2}(G_\mathrm{M}^\psi - G_\mathrm{E}^\psi)Q_\mu\right], \tag{4}$$

where G_M is the magnetic form factor, G_E is the electric form factor, and the Λ-decay distributions in the Λ-rest system are evaluated such that

$$|M(\Lambda(s_1)\to p\pi^-)|^2 = R_\Lambda[1+\alpha_1\hat{\boldsymbol{l}}_1\cdot\boldsymbol{n}_1], \tag{5}$$

$$|M(\bar{\Lambda}(s_2)\to \bar{p}\pi^+)|^2 = R_\Lambda[1+\alpha_2\hat{\boldsymbol{l}}_2\cdot\boldsymbol{n}_2], \tag{6}$$

where $\hat{\boldsymbol{l}}_1(\hat{\boldsymbol{l}}_2)$ is the unit vector in the direction of the proton (antiproton) momentum in the $\Lambda(\bar{\Lambda})$-rest frame. α_1 and α_2 are the decay asymmetry parameters for $\Lambda\to p\pi^-$ and $\bar{\Lambda}\to\bar{p}\pi^+$. R_Λ is determined by the Λ decay rate.

Using the folding method[28], the whole decay cross-section embedded in the subsequent hyperon decay processes is formed as

$$\begin{aligned}|M|^2 = \sum_{\pm s_1,\pm s_2} &< |M(e^+e^-\to\Lambda(s_1)\bar{\Lambda}(s_2))|^2\cdot \\ &|M(\Lambda(s_1)\to p\pi^-)|^2|M(\bar{\Lambda}(s_2)\to\bar{p}\pi^+)|^2 >_{n_1n_2},\end{aligned} \tag{7}$$

where $\langle\,\rangle_{n_1n_2}$ represents the average over the spin-quantization directions.

Integrating all the information mentioned above, we can obtain $\mathrm{d}\sigma \propto W(\xi)\mathrm{d}\cos\theta\mathrm{d}\Omega_1\mathrm{d}\Omega_2$, where the joint angular distribution $W(\xi)$ is

$$\begin{aligned}\mathcal{W}(\xi) = &F_0(\xi)+\alpha_\psi F_5(\xi)+\alpha_1\alpha_2(F_1(\xi)+ \\ &\sqrt{1-\alpha_\psi^2}\cos(\Delta\Phi)F_2(\xi)+\alpha_\psi F_6(\xi))+ \\ &\sqrt{1-\alpha_\psi^2}\sin(\Delta\Phi)(\alpha_1F_3(\xi)+\alpha_2F_4(\xi)),\end{aligned} \tag{8}$$

which retains only the components that determine the angular distribution of the cross-section regardless of the angle-independent factor. $\Delta\Phi$ is the relative phase between the form factors G_E^ψ and G_M^ψ. α_ψ is the ratio of the form factors constructed as

$$\alpha_\psi = \frac{s|G_M^\psi|^2 - 4M^2|G_E^\psi|^2}{s|G_M^\psi|^2 + 4M^2|G_E^\psi|^2}, \tag{9}$$

where M is the Λ mass and $s=(p_1+p_2)^2$. The seven $F_k(\xi)$ functions are defined as

$$\begin{aligned}&F_0(\xi)=1,\\ &F_1(\xi)=\sin^2\theta\sin\theta_1\sin\theta_2\cos\phi_1\cos\phi_2+\cos^2\theta\cos\theta_1\cos\theta_2,\\ &F_2(\xi)=\sin\theta\cos\theta(\sin\theta_1\cos\theta_2\cos\phi_1+\cos\theta_1\sin\theta_2\cos\phi_2),\\ &F_3(\xi)=\sin\theta\cos\theta\sin\theta_1\sin\phi_1,\\ &F_4(\xi)=\sin\theta\cos\theta\sin\theta_2\sin\phi_2,\\ &F_5(\xi)=\cos^2\theta,\\ &F_6(\xi)=\cos\theta_1\cos\theta_2-\sin^2\theta\sin\theta_1\sin\theta_2\sin\phi_1\sin\phi_2,\end{aligned} \tag{10}$$

where $\xi=\xi(\theta,\Omega_1,\Omega_2)$ with θ is the scattering angle of Λ in the c.m. system. $\Omega_1=(\theta_1,\phi_1)$ is the spherical angle for the proton in the Λ-rest frame, and $\Omega_2=(\theta_2,\phi_2)$ is the spherical angle for the anti-proton in the $\bar{\Lambda}$-rest frame. Fig. 1 shows the coordinate system with the angles mentioned above. The concrete coordinate system with basis vectors is defined as

$$\begin{aligned}\boldsymbol{e}_x &= \frac{1}{\sin\theta}(\hat{\boldsymbol{p}}\times\hat{\boldsymbol{k}})\times\hat{\boldsymbol{p}},\\ \boldsymbol{e}_y &= \frac{1}{\sin\theta}(\hat{\boldsymbol{p}}\times\hat{\boldsymbol{k}}),\\ \boldsymbol{e}_z &= \hat{\boldsymbol{p}},\end{aligned} \tag{11}$$

where the scattering plane with the vectors $\boldsymbol{p}$ and $\boldsymbol{k}$ makes up the xz-plane, with the y-axis along the normal to the scattering plane. The polarization is in the $\boldsymbol{e}_y$ direction and is expressed in Eq. (2). The polarization occurs when the phase

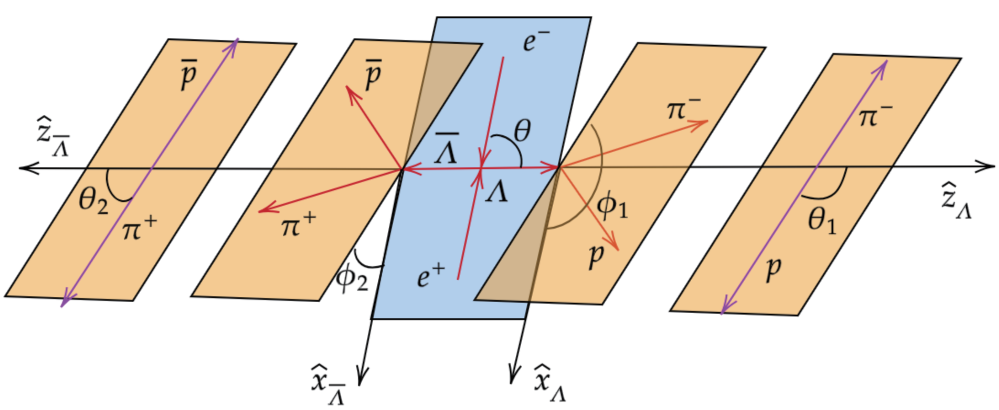

Fig. 1. The helicity frame and helicity angle in the decay $e^+e^-\to\Lambda\bar{\Lambda}\to p\pi^-\bar{p}\pi^+$.

CSTR: 32290.14.JUSTC-2024-0072
DOI: 10.52396/JUSTC-2024-0072
JUSTC, **2025**, 55(4): 0405

$\Delta\Phi$ is not equal to 0.

4 Reconstruction of $J/\psi \to Y\bar{Y}$

In this analysis, two decay channels, $J/\psi \to \Lambda\bar{\Lambda}$ and $J/\psi \to \Xi^-\bar{\Xi}^+$ with $\Lambda \to p\pi^-$ and $\Xi^- \to \Lambda\pi^- \to p\pi^-\pi^-$, are used as benchmark processes to study the reconstruction of hyperons. A brief event selection is introduced based on the general designed detector as discussed in Section 2. Charged tracks detected in the MDC are required to be within a polar angle (θ) range of detector acceptance, $|\cos\theta| < 0.93$, where θ is the polar angle with respect to the z-axis. Owing to the long-life of Λ and Ξ^-, they are likely to travel for a long path before decay. Thus no requirement for the distance of the closest approach to the interaction point for charged tracks is applied. Events with at least 4 and 6 charged tracks are retained in the physical processes $J/\psi \to \Lambda\bar{\Lambda}$ (referred to as the Λ channel) and $J/\psi \to \Xi^-\bar{\Xi}^+$ (referred to as the Ξ channel). Based on the kinematic characteristics, tracks with momentum greater than 0.5 (0.32) GeV/c are considered as proton candidates, otherwise, as pion candidates for Λ channel (Ξ channel). There are no further particle identification requirements. Only events with at least one proton, one antiproton, two pions with opposite charges (one proton, one anti-proton, two negative and two positive charged pions) are saved for further analysis for Λ channel (Ξ channel). To reconstruct the correct Λ and Ξ for these two channels, vertex fits are performed. To find the correct Λ candidate in Λ channel, all combinations with proton and π^- candidates are looping to perform vertex fit. Events with minimum χ^2 lower than 200, decay length larger than 0 and the cut on $m_{p\pi^-}$ mass window within five times the mass resolution are selected as Λ candidates. The same procedure is performed for the $\bar{\Lambda}$ decay chain. For $\Xi^- \to \Lambda\pi^- \to p\pi^-\pi^-$ decay, the Λ and Ξ^- particles are reconstructed through vertex fits by first combining the $p\pi_i^-$ pair to form a Λ and then the $\Lambda\pi_j^-$ $(i \neq j)$ pair to form a Ξ^-. Events with minimum $\sqrt{(m_{p\pi\pi} - M_\Xi)^2 + (m_{p\pi} - M_\Lambda)^2}$, decay length greater than 0 and the mass window cut corresponding to five times mass resolution for both Ξ and Λ are selected, where M_Ξ and M_Λ are the nominal masses quoted from particle data group (PDG)[19] and $m_{p\pi\pi}(m_{p\pi})$ is the invariant mass of the candidate $\Xi(\Lambda)$. The same procedure is performed for the $\bar{\Xi}$ decay chain.

Two kinds of vertex fit packages are provided officially based on different treatments on helix tracks. The default helix track reconstruction considers the energy-loss effect from the initial point (IP) to the first hit layer which is the beampipe, while the other one doesn’t. For long-life particles with secondary decays, the reconstructed vertex would be unreliable when the default helix track is used because the decay points are far away from the IP, thus a way called refined vertex fit could reduce such systematic deviation by using appropriate helix tracks according to the positions of the reconstructed vertex and their relationships with the beampipe within the inner MDC wall. Explicit indications of such influence on the reconstructed invariant mass are illustrated in Fig. 2. Using the refined vertex fit, the impact of above effects on reconstructed mass is suppressed. Considering the process $\Xi \to p\pi^-\pi^-$ the corresponding results are shown in Fig. 3. It is found that the energy loss has a tiny effect on the angular distribution but a large effect on the momentum. The refined method is effective for correcting the detected proton momentum.

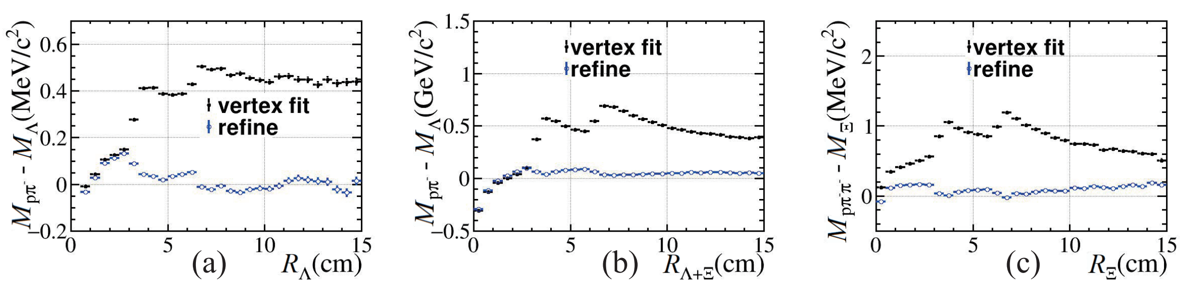

Fig. 2. The distribution of the resolution of the reconstructed masses of Λ and Ξ. (a) The resolution of Λ with respect to the decay length of Λ in the process $J/\psi \to \Lambda\bar{\Lambda} \to p\pi^-\bar{p}\pi^+$, (b) the resolution of Λ with respect to the sum decay length of Ξ and Λ in process $J/\psi \to \Xi(\to \Lambda\pi^-)\bar{\Xi}(\to \bar{\Lambda}\pi^+) \to p\pi^-\pi^-\bar{p}\pi^+\pi^+$, and (c) the resolution of the reconstructed mass of Ξ with respect to the decay length of Ξ in process $J/\psi \to \Xi(\to \Lambda\pi^-)\bar{\Xi}(\to \bar{\Lambda}\pi^+) \to p\pi^-\pi^-\bar{p}\pi^+\pi^+$. The black points represent the resolutions after secondary vertex fit while the blue points refer to the refined value of the former.

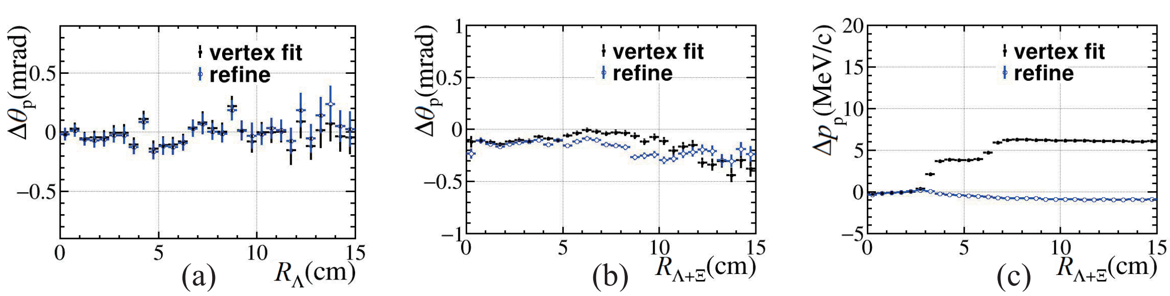

Fig. 3. The resolution of the reconstructed momenta and angles. (a) The resolution of the polar angle for proton with respect to the decay length of Λ in process $J/\psi \to \Lambda\bar{\Lambda} \to p\pi^-\bar{p}\pi^+$. (b) and (c) The resolution of the polar angle and momentum for proton with respect to the sum decay length of Λ and Ξ in process $J/\psi \to \Xi(\Lambda\pi^-)\bar{\Xi}(\bar{\Lambda}\pi^+) \to p\pi^-\pi^-\bar{p}\pi^+\pi^+$, and the black point represent the resolutions after secondary vertex fit whereas the blue points refer to the refined value of the former separately.

CSTR: 32290.14.JUSTC-2024-0072
DOI: 10.52396/JUSTC-2024-0072
JUSTC, **2025**, 55(4): 0405

5 Input-output check with different resolutions

A possible source of systematic uncertainty in the hyperon CPV probe arises from the effects of position resolution and momentum resolution. The MC sample based on the GEANT4-free fast simulation package with event selection efficiencies is used in this section. The sensitivities to these sources are investigated by performing an input-output (IO) check of the angular distribution parameters (α_ψ, $\Delta\Phi$, α_1, α_2), where α_1 and α_2 are the decay parameters of $\Lambda \to p\pi^-$ and $\bar{\Lambda} \to \bar{p}\pi^+$. With the flexible interface of fast simulation package, the simulated position resolution and momentum resolution were uniformly improved from 1 time to 1/10 times of the original value separately.

To extract the parameters, unbinned maximum-likelihood fits using samples with different position resolutions and different momentum resolutions are performed on the joint angular distributions. The probability density function of the ith event is defined by

$$\mathcal{P}(\boldsymbol{\xi}_i;\omega) = \frac{\mathcal{W}(\boldsymbol{\xi}_i;\omega)}{\mathcal{N}(\omega)}, \tag{12}$$

where $\mathcal{W}(\boldsymbol{\xi}_i;\omega)$ is the anger distribution function shown in Eq. (8), $\boldsymbol{\xi}_i = \boldsymbol{\xi}_i(\theta,\Omega_1,\Omega_2)$ is the angular vector, $\omega = \omega(\alpha_\psi,\Delta\Phi,\alpha_1,\alpha_2)$ represents the angular distribution parameters, and $\mathcal{N}(\omega) = \int \mathcal{W}(\boldsymbol{\xi};\omega)\mathrm{d}\boldsymbol{\xi}$ is the normalization factor. By introducing a specific distribution function $\mathcal{F}$, the integration can also be expressed as

$$\mathcal{N}(\omega) = \int \frac{\mathcal{W}(\xi;\omega)}{\mathcal{F}(\boldsymbol{\xi};\omega_{\text{input}})}\mathcal{F}(\boldsymbol{\xi};\omega_{\text{input}})\mathrm{d}\boldsymbol{\xi}. \tag{13}$$

In our case this specific distribution function $\mathcal{F}$ is the same as that of the integration MC sample $\mathcal{W}$. The numerical integral is performed via the approximation

$$\mathcal{N}(\omega) = \frac{1}{CM}\sum_{j=1}^{M}\frac{\mathcal{W}(\boldsymbol{\xi}_j;\omega)}{\mathcal{W}(\boldsymbol{\xi}_j;\omega_{\text{input}})}, \tag{14}$$

where M represents the number of integration MC events, and C is the normalization constant of the integral of $\mathcal{W}(\boldsymbol{\xi};\omega_{\text{input}})$ which is irrelevant to the minimization of the likelihood function and can be dropped out directly. The corresponding likelihood function is

$$\mathcal{L}(\boldsymbol{\xi}_i;\omega) = \prod_{i=1}^{N}\mathcal{P}(\boldsymbol{\xi}_i;\omega) = \prod_{i=1}^{N}\frac{\mathcal{W}(\boldsymbol{\xi}_i;\omega)}{\mathcal{N}(\omega)}, \tag{15}$$

where N is the observed number of events. Usually, the minimization of $-\ln\mathcal{L}$ is performed via the MINUIT package,

$$-\ln\mathcal{L}(\boldsymbol{\xi}_i;\omega) = -\sum_{i=1}^{N}\ln\mathcal{P}(\boldsymbol{\xi}_i;\omega) = -\sum_{i=1}^{N}\ln\mathcal{W}(\boldsymbol{\xi}_i;\omega) + \ln\mathcal{N}(\omega). \tag{16}$$

Each generated sample passes the fast simulation software with a fixed position resolution or momentum resolution as previously introduced, and is further divided into 10 sub-samples evenly. Thus, the 100 subsamples, with 10 categorized in a group since they have the same resolution, are used in the following IO check procedure. Each subsample is treated as pseudo-data and will be fitted with the procedure introduced above. For the calculation of MC integration $\mathcal{N}$, the total sample is used when the resolution of the MC integration sample is different from that of the data, and the other nine subsamples are combined and used when the resolutions are the same between the MC integration sample and pseudo-data. Therefore, all fits are organized in two large $10\times10\times10$ cycles for the IO check under different position resolutions and momentum resolutions.

During each fit, an IO check is carried out by calculating $\chi_{ijk} = \frac{\omega_{ijk}-\omega_{\text{input}}}{\sigma_{ijk,\text{stat}}}$, where i denotes the pseudo-data that used to calculate $\mathcal{W}$, j denotes the resolution of the MC integration sample used to calculate $\mathcal{N}$, and k is the label of the subsample sequence in the total sample with a given resolution. ω_{ijk} is the fit result of the parameters, ω_{input} is the input quantity and $\sigma_{ijk,\text{stat}}$ is the corresponding statistical uncertainty. Then the quantities

$$\chi_{ij} = \frac{1}{10}\left|\sum_{k=1}^{10}\chi_{ijk}\right| = \frac{1}{10}\left|\sum_{k=1}^{10}\frac{\omega_{ijk}-\omega_{\text{input}}}{\sigma_{ijk,\text{stat}}}\right| \tag{17}$$

are treated as the sensitive quantities for testing the detector capabilities.

The results of χ_{ij} are summarized in Fig. 4 for the position resolution IO test and in Fig. 5 for the momentum resolution IO test. The labels on the axes indicate the samples used with the given resolutions, for example in Fig. 4, res0.1 indicates that the sample with position resolution improved to 0.1 times the original value. On the diagonal of each plot, the resolution of the pseudo-data is the same as that of the integration MC, but different in the off-diagonal region. The fit results indicate that, whether for position resolution or for momentum resolution, a systematic deviation will be introduced if the resolution of the MC integration samples used for calculating the numerical integral is different from that of the pseudo-data sample, and the bias increases as the resolution difference incerases.

6 Conclusions

In this paper, the reconstruction of hyperons and the parameters that construct CPV observables of hyperon decay based on the effects of energy-loss and detector resolutions are discussed. The results provide several requirements on the tracking system designed at STCF. First, the reconstruction methods of the Λ and Ξ hyperons are discussed, where the different treatments on the helical tracks greatly influence the mass or angular reconstruction of the hyperons. Thus, it is necessary to reconstruct the decay points of the hyperons with high precision. An inner vertex detector at STCF will helps improve the resolution of the decay point of hyperons. Second, the IO checks of the CPV related parameters are performed under different detector resolutions. It is found that only when the MC simulation with correct position/momentum resolution compared to data, the IO on the parameters is unbiased. Otherwise, it will introduce a systematic deviation of the

CSTR: 32290.14.JUSTC-2024-0072
DOI: 10.52396/JUSTC-2024-0072
JUSTC, **2025**, 55(4): 0405

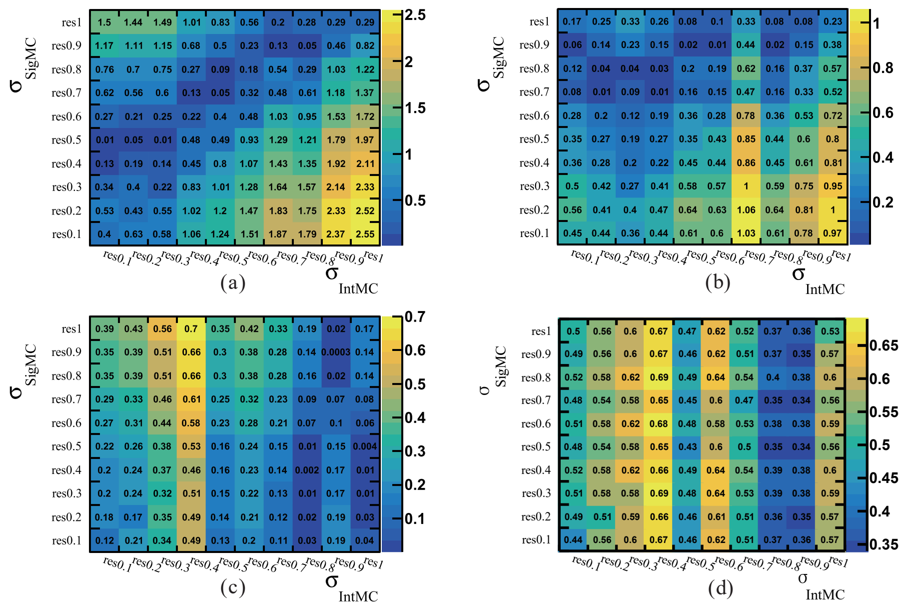

Fig. 4. Distribution of IO checks for the parameters with various position resolutions on the pseudo-data samples, denoted as $\sigma_{\rm SigMC}$ and the integration MC samples $\sigma_{\rm IntMC}$, (a) for α_ψ, (b) for $\Delta\Phi$, (c) for α_1, and (d) for α_2. The quantities in the boxes represent χ_{ij}, where i and j denote the vertical sequence and horizontal sequence.

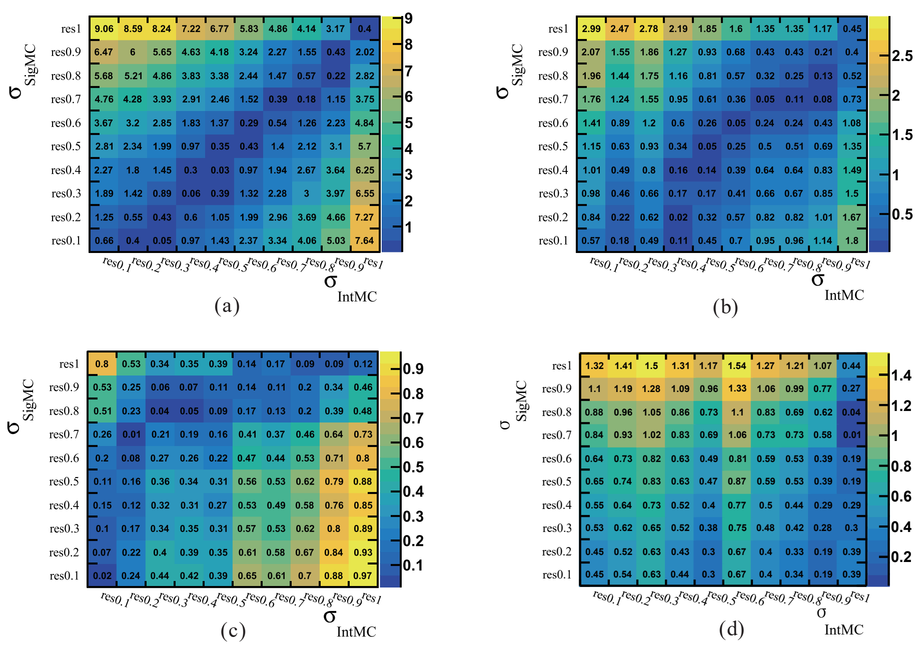

Fig. 5. Distribution of IO checks for the parameters with various momentum resolutions on pseudo-data samples, denoted as $\sigma_{\rm SigMC}$ and the integration MC samples $\sigma_{\rm IntMC}$, (a) for α_ψ, (b) for $\Delta\Phi$, (c) for α_1, and (d) for α_2. The quantities in the boxes represent χ_{ij}, where i and j denote the vertical sequence and horizontal sequence.

final results. This requires a careful estimation of the data/MC difference in tracking reconstruction at future STCF.

Notably, systematic uncertainty is not inclusively discussed in this paper, as there are more effects that will cause systematic uncertainties. One example is the magnetic field non-uniformity, which could cause 10^{-4} uncertainty as has been discussed in Ref. [29]. Another effect could be the regeneration or the decoherence effects, in which the hyperons interact with the material in the detector. A complete systematic uncertainty can be real only with the operation of the detector. This study provides the first attempt to study the possible systematic sources from the detector aspects that will be used to guide the design of the STCF detector.

Acknowledgements

We thank the Supercomputing Center of the University of Science and Technology of China (USTC) and the Hefei Comprehensive National Science Center for their strong support. This work was supported by the National Key R&D

CSTR: 32290.14.JUSTC-2024-0072
DOI: 10.52396/JUSTC-2024-0072
JUSTC, **2025**, 55(4): 0405

Program of China (2022YFA1602200) and the International Partnership Program of the Chinese Academy of Sciences (211134KYSB20200057).

Conflict of interest

The authors declare that they have no conflict of interest.

Biography

Ming Xu is a master student in Particle and Nuclear Physics at the University of Science and Technology of China. He received his Bachelor's degree in Applied Physics from Northeastern University in 2020. His research mainly focuses on experimental high energy physics at BESIII.

References

[1] Noether E. Invariant variation problems. *Transport Theory and Statistical Physics*, **1971**, *1*: 186–207.
[2] Sakharov A D. Violation of *CP* in variance, *C* asymmetry, and baryon asymmetry of the universe. *Soviet Physics Uspekhi*, **1991**, *34*: 392–393.
[3] Cabibbo N. Unitary symmetry and leptonic decays. *Physical Review Letters*, **1963**, *10*: 531–533.
[4] Kobayashi M, Maskawa T. *CP*-violation in the renormalizable theory of weak interaction. *Progress of Theoretical Physics*, **1973**, *49*: 652–657.
[5] Christenson J H, Cronin J W, Fitch V L, et al. Evidence for the 2π decay of the K_2^0 meson. *Physical Review Letters*, **1964**, *13*: 138.
[6] Aaij R, Abellan Beteta C, Adeva B, et al. First observation of *CP* violation in the decays of B_s^0 mesons. *Physical Review Letters*, **2013**, *110*: 221601.
[7] Aaij R, Abellan Beteta C, Adeva B, et al. Observation of *CP* violation in charm decays. *Physical Review Letters*, **2019**, *122*: 211803.
[8] Barr S, Segrè G, Weldon H A. Magnitude of the cosmological baryon asymmetry. *Physical Review D*, **1979**, *20*: 2494–2498.
[9] Donoghue J F, He X G, Pakvasa S. Hyperon decays and *CP* nonconservation. *Phys Rev D*, **1986**, *34*: 833
[10] Tandean J, Valencia G. *CP* violation in hyperon nonleptonic decays within the standard model. *Physical Review D*, **2003**, *67*: 056001.
[11] Lu C D, Wang Y M, Zou H, et al. Anatomy of the pQCD approach to the baryonic decays $\Lambda_b \to p\pi, pK$. *Physical Review D*, **2009**, *80*: 034011.
[12] Hsiao Y K, Geng C Q. Direct *CP* violation in Λ_b decays. *Physical Review D*, **2015**, *91*: 116007.
[13] Salone N, Adlarson P, Batozskaya V, et al. Study of *CP* violation in hyperon decays at super-charm-tau factories with a polarized electron beam. *Physical Review D*, **2022**, *105*: 116022.
[14] Buras A J, Kaon theory: 50 years later. arXiv: 2307.15737, **2023**.
[15] Lee T D, Yang C N. General partial wave analysis of the decay of a hyperon of spin ½. *Physical Review*, **1957**, *108*: 1645–1647.
[16] He X G, Tandean J, Valencia G. Pursuit of *CP* violation in hyperon decays at e^+e^- colliders. *Science Bulletin*, **2022**, *67*: 1840–1843.
[17] The BESIII Collaboration. Polarization and entanglement in baryon–antibaryon pair production in electron–positron annihilation. *Nature Physics*, **2019**, *15*: 631–634.
[18] Achasov M, Ai X C, An L P, et al. STCF conceptual design report (Volume 1): physics & detector. *Frontiers of Physics*, **2024**, *19*: 14701.
[19] Particle Data Group and others. Review of particle physics. *Progress of Theoretical and Experimental Physics*, **2022**, *2022*: 083C01.
[20] The BESIII Collaboration. Precise measurements of decay parameters and *CP* asymmetry with entangled $\Lambda\bar{\Lambda}$ pairs. *Physical Review Letters*, **2022**, *129*: 131801.
[21] The BESIII Collaboration. Test of *CP* symmetry in hyperon to neutron decays. *Physical Review Letters*, **2023**, *131*: 191802.
[22] The BESIII Collaboration. Tests of *CP* symmetry in entangled $\Xi^0 - \bar{\Xi}^0$ pairs. *Physical Review D*, **2023**, *108*: L031106.
[23] The BESIII Collaboration. Probing *CP* symmetry and weak phases with entangled double-strange baryons. *Nature*, **2022**, *606*: 64–69.
[24] Xu Y, Zhou X, Shi X, et al. Sensitivity of CP violation of Λ decay in $J/\psi \to \Lambda\bar{\Lambda}$ at STCF. *Modern Physics Letters A*, **2022**, *37*: 2250208.
[25] Zeng S, Xu Y, Zhou X R, et al. Prospects of *CP* violation in Λ decay with a polarized electron beam at the STCF. *Chinese Physics C*, **2023**, *47*: 113001.
[26] Shi X D, Zhou X R, Qin X S, et al. A fast simulation package for STCF detector. *Journal of Instrumentation*, **2021**, *16*: P03029.
[27] Fäldt G, Kupsc A. Hadronic structure functions in the $e^+e^- \to \Lambda\bar{\Lambda}$ reaction. *Physics Letters B*, **2017**, *772*: 16–20.
[28] Fäldt G. Entanglement in joint $\Lambda\bar{\Lambda}$ decay. *The European Physical Journal A*, **2015**, *51*: 74.
[29] Li H B, Ma X X. Polarization difference between hyperons and antihyperons induced by an external magnetic field. *Physical Review D*, **2019**, *100*: 076007.

CSTR: 32290.14.JUSTC-2024-0072
DOI: 10.52396/JUSTC-2024-0072
JUSTC, **2025**, 55(4): 0405